Available online at www.sciencedirect.com
ScienceDirect
Journal of Solid State Chemistry 180 (2007) 1171–1179
JOURNAL OF SOLID STATE CHEMISTRY
www.elsevier.com/locate/jssc

The role of anhydrous zinc nitrate in the thermal decomposition of the zinc hydroxy nitrates $Zn_5(OH)_8(NO_3)_2 \cdot 2H_2O$ and $ZnOHNO_3 \cdot H_2O$

Timothy Biswick[a], William Jones[a,*], Alexandra Pacuła[b], Ewa Serwicka[b], Jerzy Podobinski[b]

[a]*Department of Chemistry, University of Cambridge, Lensfield Road, Cambridge CB2 1EW, UK*
[b]*Institute of Catalysis and Surface Chemistry, Polish Academy of Sciences, ul. Niezapominajek 8, 30-329 Krakow, Poland*

Received 18 October 2006; received in revised form 6 January 2007; accepted 15 January 2007
Available online 24 January 2007

Abstract

The steps associated with the thermal decomposition of $Zn_5(OH)_8(NO_3)_2 \cdot 2H_2O$ and $ZnOHNO_3 \cdot H_2O$ are re-examined. Previous reports have suggested that $Zn_5(OH)_8(NO_3)_2 \cdot 2H_2O$ decomposes to ZnO via two intermediates, $Zn_5(OH)_8(NO_3)_2$ and $Zn_3(OH)_4(NO_3)_2$ whereas $ZnOHNO_3 \cdot H_2O$ has been reported to decompose to ZnO via a $Zn_3(OH)_4(NO_3)_2$ intermediate. In this study, we demonstrate using TG, mass spectral analysis of evolved gases and *in situ* variable temperature powder X-ray diffraction analysis that, in fact, in the decomposition of $Zn_5(OH)_8(NO_3)_2 \cdot 2H_2O$ an anhydrous zinc nitrate intermediate is also involved. We, additionally, show that the decomposition of $ZnOHNO_3 \cdot H_2O$ to ZnO also involves the formation of an anhydrous zinc nitrate intermediate. The anhydrous zinc nitrate formed in both cases is poorly crystallised and this observation may explain why this phase could not be observed by PXRD analysis in the previous studies.

Keywords: Zinc hydroxy nitrates; Thermal decomposition; Anhydrous zinc nitrate; Evolved gases mass spectral analysis; ZnO

1. Introduction

Layered double hydroxides (LDHs) and hydroxy salts form a family of inorganic layered solids attracting ever increasing attention. The ability to vary the intralayer metal composition, as well as the identity of the interlayer anions, renders these materials attractive substrates for advanced materials design for a broad range of applications. The reported applications of these materials include the preparation of anion exchangers, complex organic–inorganic hybrid materials, and the slow release drug delivery agents [1–7].

An additional important characteristic of these solids is the topotactic nature of the processes accompanying their thermal decomposition to oxides, which allows for the preparation of oxidic nanoparticles with unique sorptive, catalytic, magnetic or electric properties [8,9]. Novel materials based on microcrystalline ZnO are of particular interest in view of the low toxicity of ZnO and a wide range of possible applications, including solar cell technology, catalysis and photo-catalysis, thin-film gas sensors, varistors, transparent conductive electrodes and surface acoustic wave devices [10,11]. Several recent reports have recognised hydroxy salts of zinc as exceptionally promising precursors of nano-textured ZnO particles for electronics and optoelectronics [12–16].

For a proper control of the properties of the end product, however, a detailed knowledge of the thermal decomposition process of appropriate precursors is essential. Analysis of the literature data, however, shows that, as far as the thermal decomposition of hydroxy salts is concerned, this area of research is fragmentary and contains considerable gaps or omissions. In this paper, we address this issue for two zinc hydroxy nitrates $Zn_5(OH)_8(NO_3)_2 \cdot 2H_2O$ and $ZnOHNO_3 \cdot H_2O$.

The structure of $Zn_5(OH)_8(NO_3)_2 \cdot 2H_2O$ belongs to type IIb according to the classification of Louër et al. [17]. It consists of infinite brucite-like layers, where one quarter of the octahedrally coordinated zinc atom sites are vacant and on either side of the empty octahedra there are zinc atoms tetrahedrally coordinated by OH groups (forming the base

*Corresponding author. Fax: +44 1223 336 362.
E-mail address: wj10@cam.ac.uk (W. Jones).

0022-4596/$ - see front matter © 2007 Elsevier Inc. All rights reserved.
doi:10.1016/j.jssc.2007.01.012

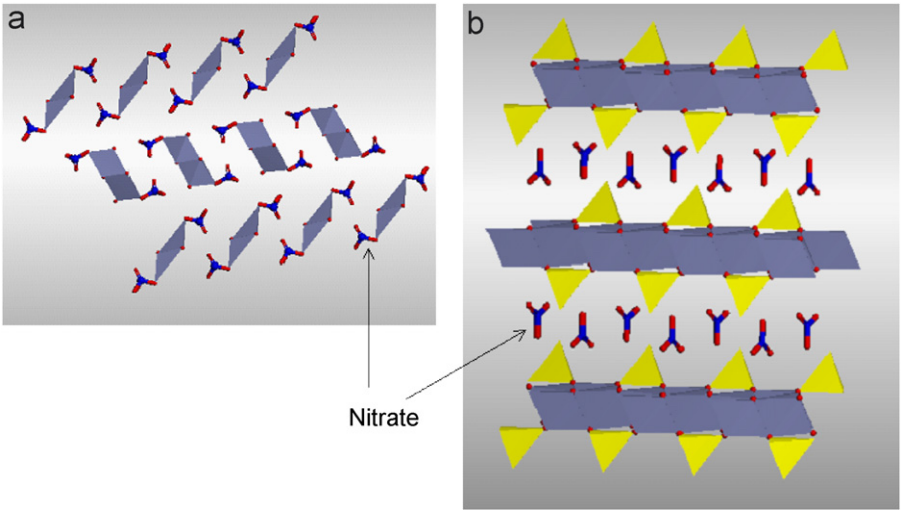

Fig. 1. Schematic representation of the structures of (a) $ZnOHNO_3 \cdot H_2O$ and (b) $Zn_5(OH)_8(NO_3)_2 \cdot 2H_2O$ showing coordinated and free nitrate, respectively.

$$Zn_5(OH)_8(NO_3)_2.2H_2O \xrightarrow{80\text{ - }120\ ^\circ C} Zn_5(OH)_8(NO_3)_2 + 2H_2O \quad (1)$$

$$Zn_5(OH)_8(NO_3)_2 \xrightarrow{120\text{ - }140\ ^\circ C} Zn_3(OH)_4(NO_3)_2 + 2ZnO + 2H_2O \quad (2)$$

$$Zn_3(OH)_4(NO_3)_2 \xrightarrow{140\text{ - }170\ ^\circ C} 3ZnO + 2HNO_3 + H_2O \quad (3)$$

Fig. 2. Reaction steps during the decomposition of $Zn_5(OH)_8(NO_3)_2 \cdot 2H_2O$ as proposed by Auffredic and Louër [20].

of a tetrahedron), with a water molecule occupying the apex. Unbound nitrate groups are located between the sheets (Fig. 1) [18]. $ZnOHNO_3 \cdot H_2O$ is not layered and consists of infinite double chains of edge sharing octahedra, in which zinc coordinates three hydroxyls, one nitrate anion and two water molecules [19].

A detailed study of the reactions associated with the thermal decomposition of $Zn_5(OH)_8(NO_3)_2 \cdot 2H_2O$ has been reported by Auffredic and Louër [20]. They proposed, on the basis of *in situ* variable temperature PXRD, TG analysis and mass spectral analysis of the evolved gases, that decomposition of the material to ZnO occurs via the following three steps (Fig. 2).

Additionally, the authors observed that whilst XRD analysis suggested that the total structural transformation of $Zn_5(OH)_8(NO_3)_2 \cdot 2H_2O$ to ZnO was complete by ca. 170 °C, the release of gaseous products (monitored by mass spectrometry) was finalised only at 300 °C. This difference they interpreted as resulting from adsorption of evolved gases on the surface of the solid product (i.e. microcrystalline ZnO) and their subsequent release at higher temperatures. Aufredic and Louër further investigated the decomposition of $ZnOHNO_3 \cdot H_2O$. They reported that it decomposes to ZnO in a two-step process via a $Zn_3(OH)_4(NO_3)_2$ phase.

A new aspect of the possible solid state transformation of $Zn_3(OH)_4(NO_3)_2$ (which is an intermediate product during the decomposition of $Zn_5(OH)_8(NO_3)_2 \cdot 2H_2O$—Fig. 2—and $ZnOHNO_3 \cdot H_2O$) has recently been raised by Malecka et al. [21]. The authors observed, from TG analysis, that $Zn_3(OH)_4(NO_3)_2$ decomposes to ZnO in two steps. Of particular importance was the fact that mass spectral analysis of the evolved gases showed that the first mass loss involved the evolution of both water and nitrogen-containing species, whereas in the second step only nitrogen-containing species were released. However, ZnO was the only crystalline phase observed from PXRD analysis in the temperature range corresponding to the end of the first step of mass loss. They proposed, therefore, that the first decomposition step of $Zn_3(OH)_4(NO_3)_2$ involved the formation of amorphous anhydrous zinc nitrate, which then decomposed to ZnO in the second step.

The objectives of the present paper are to re-examine the thermal decomposition of $Zn_5(OH)_8(NO_3)_2 \cdot 2H_2O$ and $ZnOHNO_3 \cdot H_2O$ and determine whether the $Zn_3(OH)_4(NO_3)_2$ intermediate formed from these materials also decomposes to ZnO via an amorphous anhydrous zinc nitrate phase.

2. Experimental

2.1. Materials

The preparation of $Zn_5(OH)_8(NO_3)_2 \cdot 2H_2O$ and ZnOH $NO_3 \cdot H_2O$ was performed, with some modifications, according to procedures reported by Newman and Jones [22] and Eriksson et al. [19]. $Zn_5(OH)_8(NO_3)_2 \cdot 2H_2O$ (Zn_5–H_2O hereafter) was prepared by dropwise addition, with constant stirring, of 50 ml of 0.75 M aqueous sodium hydroxide to 20 ml of 3.5 M aqueous zinc nitrate at room temperature. The precipitate was filtered, washed twice with deionised water and air dried $ZnOHNO_3 \cdot H_2O$ (Zn_1–H_2O hereafter) was prepared by heating $Zn(NO_3)_2 \cdot 6H_2O$ at 100 °C for 12 h.

2.2. Methods

The room temperature PXRD data was collected on a Philips X'Pert MPD diffractometer using CuKα radiation ($\lambda = 1.540$ Å) at 40 kV and 40 mA. The patterns were recorded from 5° to 80° 2θ with a scan step time of 19.7 s and a step size of 0.02°. Variable temperature PXRD data was collected on the Philips Diffractometer described above using an Anton Paar TTK450 Low-Temperature attachment. The patterns were collected under vacuum (ca. 10^{-2} mbar) from 8° to 40° 2θ with a scan step time of 12.1 s and a step size of 0.02°. The procedure involved heating the sample (at a heating rate of 5 °C min^{-1}) to the desired temperature and immediately start taking a PXRD scan at that temperature. Measurements were performed from 60 to 400 °C at increments of 20 °C.

TG profiles were recorded on a Mettler Toledo TGA/SDTA 851^e from 30 to 400 °C at a heating rate of 1 °C min^{-1} in flowing nitrogen (50 ml min^{-1}). Mass spectral analysis of the gases evolved during thermal decomposition was carried out for 0.05 g samples heated at the rate of 3 °C min^{-1} in flowing argon (10 ml min^{-1}) using RGA200 Stanford Research quadrupole mass spectrometer.

FTIR spectra were recorded on a ThermoNicolet Smart Golden Gate MKII single reflection ATR spectrometer from 4000 to 500 cm^{-1} at a 4 cm^{-1} resolution. All chemicals were reagent grade (Aldrich) and were used without further purification.

3. Results and discussion

3.1. Physicochemical characterisation of starting zinc hydroxynitrates

The PXRD patterns of Zn_5–H_2O and Zn_1–H_2O are compared with appropriate simulated patterns (from ICDD files) in Fig. 3, showing good agreement between the two sets of data. The PXRD data may be indexed on the basis of the monoclinic lattices with refined parameters $a = 19.50$ Å, $b = 6.25$ Å, $c = 5.53$ Å and $\beta = 93.32°$ and $a = 17.94$ Å, $b = 3.26$ Å, $c = 14.27$ Å and $\beta = 114.79°$, for Zn_5–H_2O and Zn_1–H_2O, respectively, in agreement with previously reported data [18,19]. There are, however, differences in the intensities of the reflections for the experimental and simulated patterns for Zn_1–H_2O, especially at higher 2 theta values. This is probably due to the effects of preferred orientation arising from the shape and size of the crystallites.

FTIR spectra (Fig. 4) are also in agreement with the established structures of the materials. Thus, the spectrum for Zn_5–H_2O contains OH stretching vibrations of the layer hydroxyls and water molecules in the region 3660–2900 cm^{-1} with the upper limit corresponding to free OH groups and the lower limit to OH groups involved in significant hydrogen bonding [23]. Three bands observed in this region are associated with the three types of structurally different hydroxyls. The sharp band at 3569 cm^{-1} may be assigned to stretching vibrations of OH groups not substantially involved in hydrogen bonding, the band at 3465 cm^{-1} may be assigned to vibrations of OH groups hydrogen bonded to nitrate groups whereas the broad band at ca. 3286 cm^{-1} may be assigned to stretching vibrations of OH groups of the water molecules.

In the Zn_5–H_2O lattice the nitrate anion appears as an unbound planar, symmetric species (D_{3h} symmetry), possessing four vibration frequencies, two of which are doubly degenerate: the asymmetric deformation (ν_2) near 830 cm^{-1}, the asymmetric stretch (ν_3) near 1370 cm^{-1} and the symmetric deformation (ν_4) near 723 cm^{-1} [24,25]. The band at 1370 cm^{-1} in Fig. 3 is, therefore, assigned to the asymmetric vibration of the nitrate. The other two nitrate absorptions appear at lower wavenumbers (723 cm^{-1} for ν_4 and 830 cm^{-1} for ν_2) and are not shown. Additionally, the spectrum shows a sharp absorption band at 1636 cm^{-1} which is due to the bending vibrations of the interlayer water molecules [22]. Finally the band at 1015 cm^{-1} is assigned to OH bending mode of the layer hydroxyls (δ_{Zn-OH}).

The FTIR spectrum of Zn_1–H_2O (Fig. 4b) in the region of OH stretching vibrations also contains three major absorption bands, at 3536, 3483, and 3184 cm^{-1}, in accordance with the presence of different OH environments as evidenced from the structural data [19]. The broad band centred at ca. 3184 cm^{-1} may be assigned to OH vibrations of water molecules whereas the bands at 3536 and 3483 cm^{-1} may be assigned to OH vibrations of the layer hydroxyls. The presence of structural water in this material is confirmed by the appearance of the H_2O bending vibration at 1664 cm^{-1}. In Zn_1–H_2O the characteristic set of stretching vibrations attributed to nitrate anion appears at 1420, 1338 and 1050 cm^{-1} and are assigned to the asymmetric stretch (ν_4), the symmetric stretch (ν_1) and the N–O stretch (ν_2), respectively. The nitrate bands positions are markedly different from those observed in Zn_5–H_2O. This reflects the major change in the structural environment of nitrate and lowering of its symmetry when passing from Zn_5–H_2O, where the nitrate is free, to Zn_1–H_2O, where it is coordinated to the matrix cation via M–ONO_2 bonds.

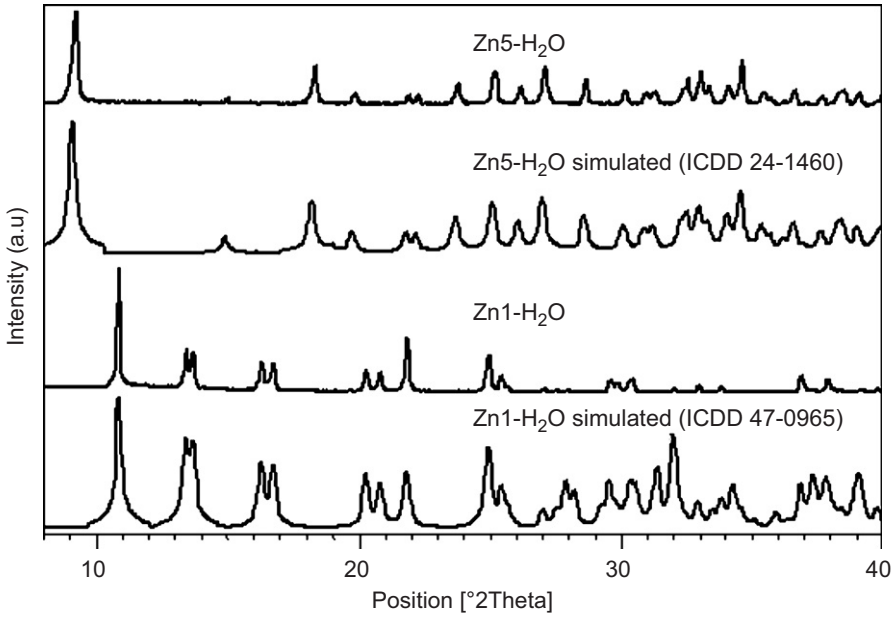

Fig. 3. Experimental and simulated X-ray diffraction patterns for Zn_5–H_2O and Zn_1–H_2O. Simulation was performed using X'Pert plus Software.

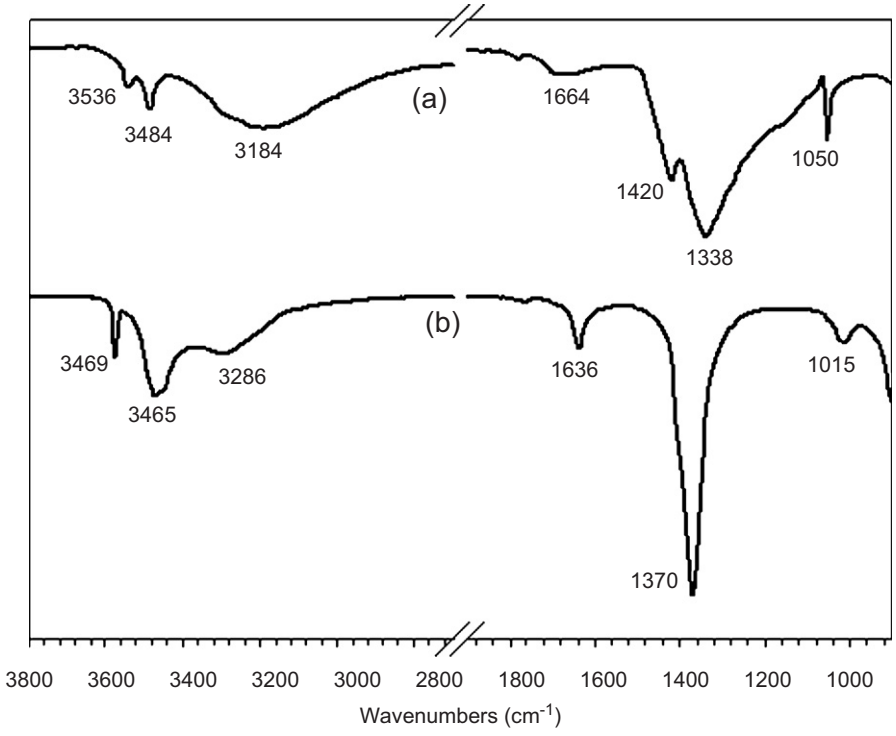

Fig. 4. FTIR spectra of (a) Zn_5–H_2O and (b) Zn_1–H_2O.

3.2. Thermal analysis

As mentioned earlier, the thermal properties of Zn_1–H_2O have previously been investigated by Auffredic et al. [20] who proposed that it decomposes to ZnO in two stages via a $Zn_3(OH)_4(NO_3)_2$ phase. Similarly, $Zn_5(OH)_8(NO_3)_2 \cdot 2H_2O$ has been shown to decompose to ZnO via a $Zn_3(OH)_4(NO_3)_2$ phase [20]. Obviously, the last steps in the decomposition of Zn_1–H_2O and Zn_5–H_2O should be similar as they involve the decomposition of the same intermediate product. Fig. 5 compares the XRD pattern of initial Zn_1–H_2O with the pattern of the same sample after heating up to 260 °C and the simulated pattern of $Zn_3(OH)_4(NO_3)_2$. Although only the strong reflections are observed, there is generally good agreement, showing that indeed $Zn_3(OH)_4(NO_3)_2$ is formed as

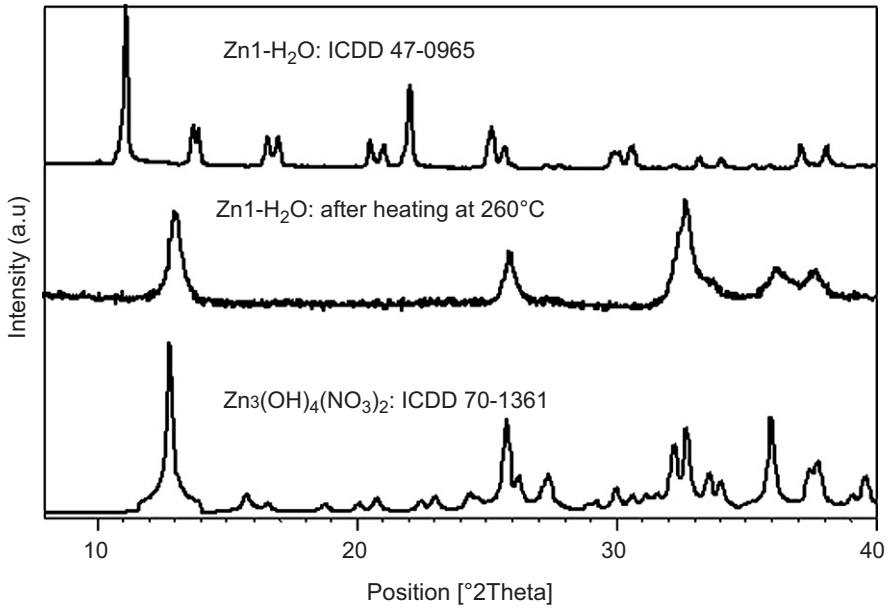

Fig. 5. PXRD patterns of Zn_1–H_2O prior to heating and after heating up to 260 °C showing the formation of $Zn_3(OH)_4(NO_3)_2$. The sample was heated at 5 °C min^{-1} to the required temperature and measurements performed *in situ* at the given temperature.

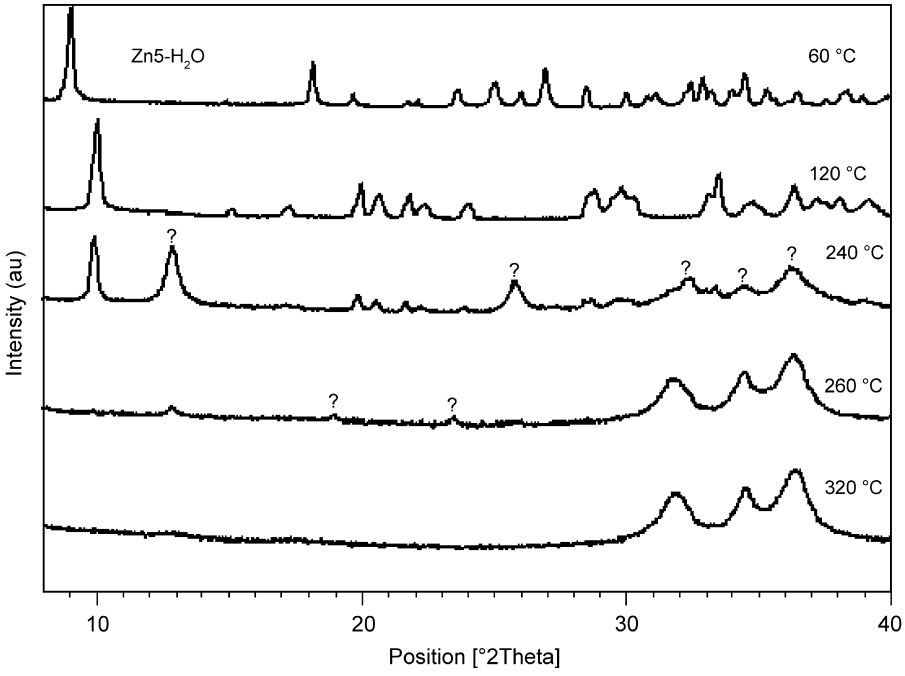

Fig. 6. The variation in the PXRD pattern of Zn_5–H_2O with temperature. ▼ = $Zn_3(OH)_4(NO_3)_2$, ◆ = unidentified phase (see text). The sample was heated at 5 °C min^{-1} to the required temperature and measurements performed *in situ* at the given temperature.

an intermediate phase during the decomposition of Zn_1–H_2O. Similarly, it is demonstrated in Fig. 6 that Zn_5–H_2O decomposes to ZnO also via $Zn_3(OH)_4(NO_3)_2$. In the present report, therefore, we will mainly focus on the thermal properties of Zn_5–H_2O, knowing that in the final stages, both Zn_5–H_2O and Zn_1–H_2O involve the decomposition of the same intermediate phase, $Zn_3(OH)_4(NO_3)_2$.

The TG and DTG profiles for Zn_5–H_2O are presented in Fig. 7 showing that the mass of the sample reaches a constant value at around 250 °C before which 4 steps of mass loss, *I, II, III and IV* are observed. The solid residue collected at the end of step *IV* was identified, by PXRD analysis, as ZnO (wurtzite structure). The observed total mass loss is 33.3% against an expected value of 34.7%, if the starting material had the ideal

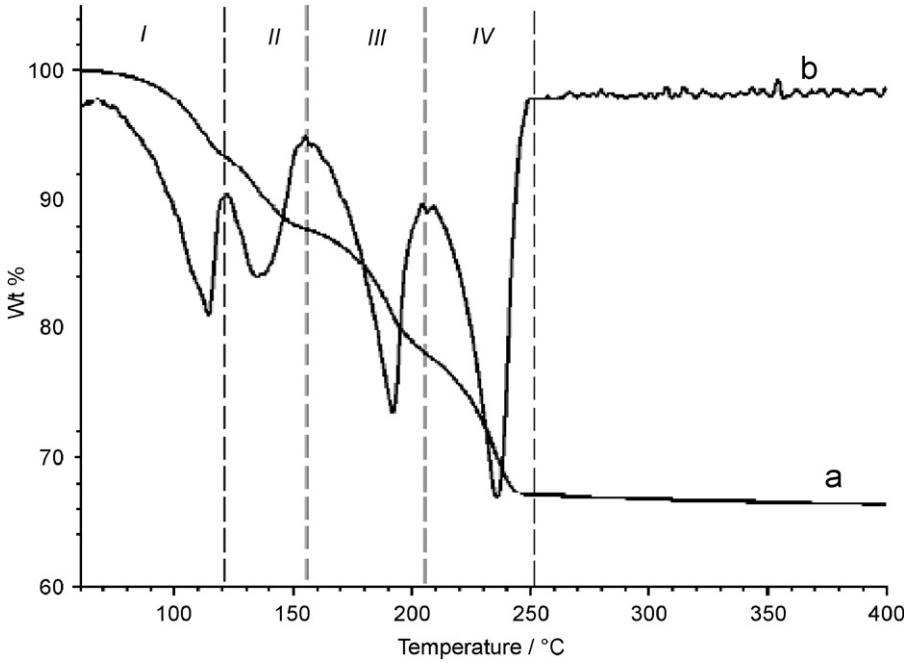

Fig. 7. (a) TG and (b) DTG profiles for Zn_5–H_2O collected for a 20 mg sample at a heating rate of 1 °C min^{-1} under flowing nitrogen (50 ml min).

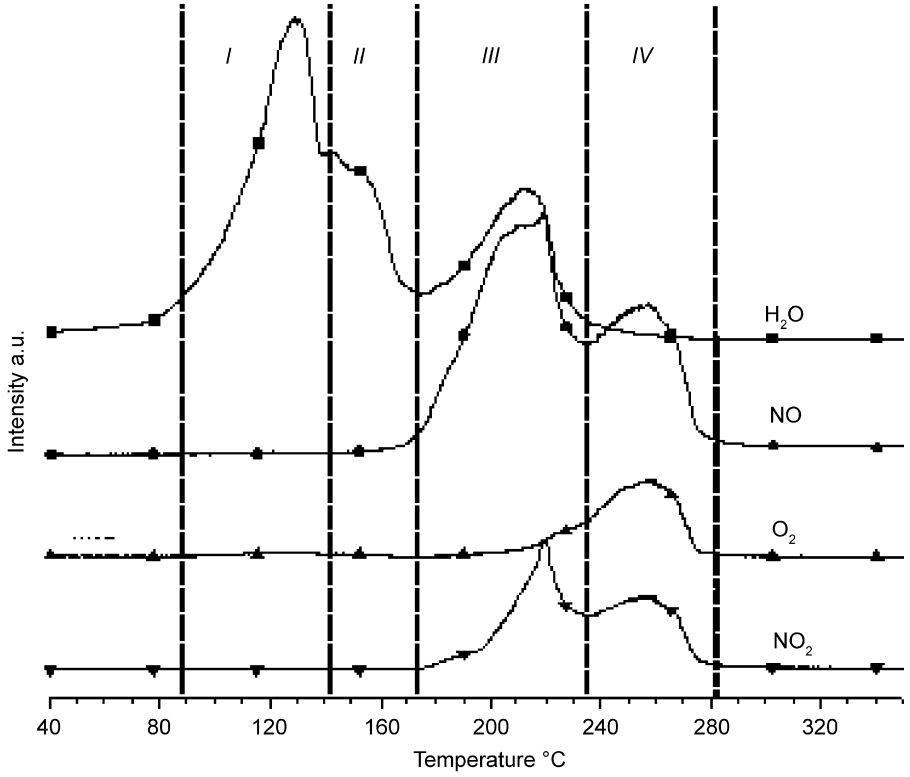

Fig. 8. Variation in ion current intensities of gaseous products released during decomposition of Zn_5–H_2O. Collected for 0.05 g sample at a heating rate of 3 °C min^{-1} in flowing argon (10 ml min^{-1}).

composition $Zn_5(OH)_8(NO_3)_2 \cdot 2H_2O$. In agreement with mass loss from the TGA data, four general temperature regions of release of gaseous products are observed by mass spectral analysis of the evolved gases (Fig. 8).

According to the reaction scheme proposed by Auffredic and Louër [20] (Fig. 2) the first two decomposition steps should account for an 11.6% mass loss (5.8% each, in both cases due to the departure of two molecules of water). Our

results indicate a 12.2% loss, close to the calculated value. It is distributed between the two steps, with 6.7% for step *I* and 5.5% for step *II*. The slight asymmetry is most likely due to the partial overlap of the dehydration process with the following dehydroxylation step. Mass spectral analysis of the evolving gases (Fig. 8) confirms that in steps *I* and *II* only water is emitted, the signal for the H_2O species evolving in two, consecutive, and partially overlapping maxima. Our results for the first two steps are, therefore, in agreement with those of Auffredic and Louër [20]. According to that study, however, the next stage involves the complete decompostion of the $Zn_3(OH)_4(NO_3)_2$ intermediate (see Eq. (3), Fig. 2) and formation of ZnO. In order to check on the suggested mechanism, it is important to analyse the evolved gas analysis profile of the material in the final stages of the decomposition. Mass spectral analysis of the gases evolved during step *III* shows that, in addition to the fragment for H_2O, fragments associated with the species NO and NO_2 also appear with significant intensity. This points to the decomposition of a nitrogen-containing species. The appearance of NO and NO_2 fragments may be indicative of the decomposition of nitrate directly to nitrogen oxides or via the decomposition of nitric acid. To distinguish between these possibilities it is necessary to analyse the profile for the species O_2. If nitrate anions were to decompose to nitrogen oxides, the gaseous products would have to contain substantial amounts of oxygen, according to the general reaction:

$$NO_3^- \rightarrow qNO + (1-q)NO + 1/4(2q+1)O_2 + 1/2O^{2-}$$

This is obviously not the case, as the O_2 signal starts to become significant only towards the end of this step (step *III*) and its maximum is associated with step *IV*. On the other hand, the literature data on the mass spectral analysis of HNO_3 [26] show that although it does contain a signal for O_2, its intensity constitutes less than 5% of the intensity of either NO or NO_2 fragments. We regard this as a strong indication that the primary nitrogen-containing species produced at the end of step *III* is HNO_3.

In step *IV* (Fig. 8), only maxima for the signals associated with NO, NO_2 and O_2 fragments appear in the mass spectrum. The lack of a maximum associated with the species H_2O shows the solid present at the end of step *III* does not contain residual water or hydroxyls.

The variation of the PXRD pattern of the material with temperature presented in Fig. 6 shows that $Zn_5(OH)_8(NO_3)_2$ (ICDD No: 37–1371) is the only crystalline phase observed at 120 °C. This corresponds to step *I* of the decomposition process, i.e. the dehydration step. Heating the material further to 240 °C leads to a number of changes in the PXRD profiles: in addition to reflections due to $Zn_5(OH)_8(NO_3)_2$, reflections associated with $Zn_3(OH)_4(NO_3)_2$ (ICDD No: 70–1361) and ZnO phases also appear with significant intensity. At 260 °C, reflections associated with $Zn_5(OH)_8(NO_3)_2$ phase have completely disappeared whereas reflections due to $Zn_3(OH)_4(NO_3)_2$ have greatly diminished in intensity and those associated with ZnO have increased in intensity. Interestingly, the PXRD pattern at this point contains two additional reflections (marked ◆ in Fig. 6) that cannot be assigned to ZnO or $Zn_3(OH)_4(NO_3)_2$. Finally only reflections associated with ZnO remain in the pattern when the material is heated at 320 °C, showing that total decomposition has now occurred. The appearance of reflections associated with $Zn_3(OH)_4(NO_3)_2$ and ZnO at 240 °C is a result of $Zn_5(OH)_8(NO_3)_2$ undergoing dehydroxylation, i.e. step *II* of Fig. 2. The increase in intensity of reflections associated with ZnO and the decrease in intensity for reflections associated with $Zn_3(OH)_4(NO_3)_2$ at 260 °C is evidence of the decomposition of $Zn_3(OH)_4(NO_3)_2$. According to Fig. 2, ZnO is the only solid phase expected from the decomposition of $Zn_3(OH)_4(NO_3)_2$. However, our data shows the presence of two weak reflections that are not characteristic of ZnO.

In view of these observations, we, therefore, propose that step *III* (of Auffredic and Louër—Fig. 2) of the decomposition of $Zn_5(OH)_8(NO_3)_2 \cdot 2H_2O$ involves two separable process. The first of which involves the formation of anhydrous zinc nitrate (labelled ◆ in Fig. 6) and ZnO as outlined in the following reaction:

$$4Zn_3(OH)_4(NO_3)_2 \rightarrow 9ZnO + 3Zn(NO_3)_2 + 7H_2O + 2HNO_3 \quad (1a)$$

The expected mass loss for the process outlined by reaction (1a) is 10.1% against the observed value of 9.5%. The process outlined by reaction (1a), therefore, leaves the anhydrous zinc nitrate as the only solid that may decompose further in step *IV* of the thermal treatment. It is likely that the anhydrous zinc nitrate produced is not well crystallised as evidenced by the observed weak reflections. The gaseous fragments accompanying the decomposition of anhydrous zinc nitrate i.e. strong signals from NO, NO_2 and O_2, as well as the absence of H_2O, indicate a typical decomposition of nitrate anions and the process occurring in step *IV* may be described as outlined in the following reaction:

$$Zn(NO_3)_2 \rightarrow ZnO + NO_2 + NO + O_2 \quad (1b)$$

The expected mass loss for this process is 13.0% while the observed is 12.0%.

Comparison of Figs. 8 and 9 (evolved gas analysis for Zn_1–H_2O) shows that the profiles for the species NO, NO_2 and O_2 in the temperature range corresponding to the final stage of thermal treatment, where the decomposition of anhydrous zinc nitrate takes place, run in a characteristic parallel to each other. This observation supports our finding concerning the common nature of the solids present in Zn_5–H_2O and Zn_1–H_2O materials towards the end of the thermal decomposition.

The formation of anhydrous metal salts during the decomposition of layered zinc hydroxy salts has been observed before for zinc hydroxy chloride, $Zn_5(OH)_8Cl_2 \cdot H_2O$ and zinc hydroxy sulphate, $Zn_4(OH)_6SO_4 \cdot 5H_2O$.

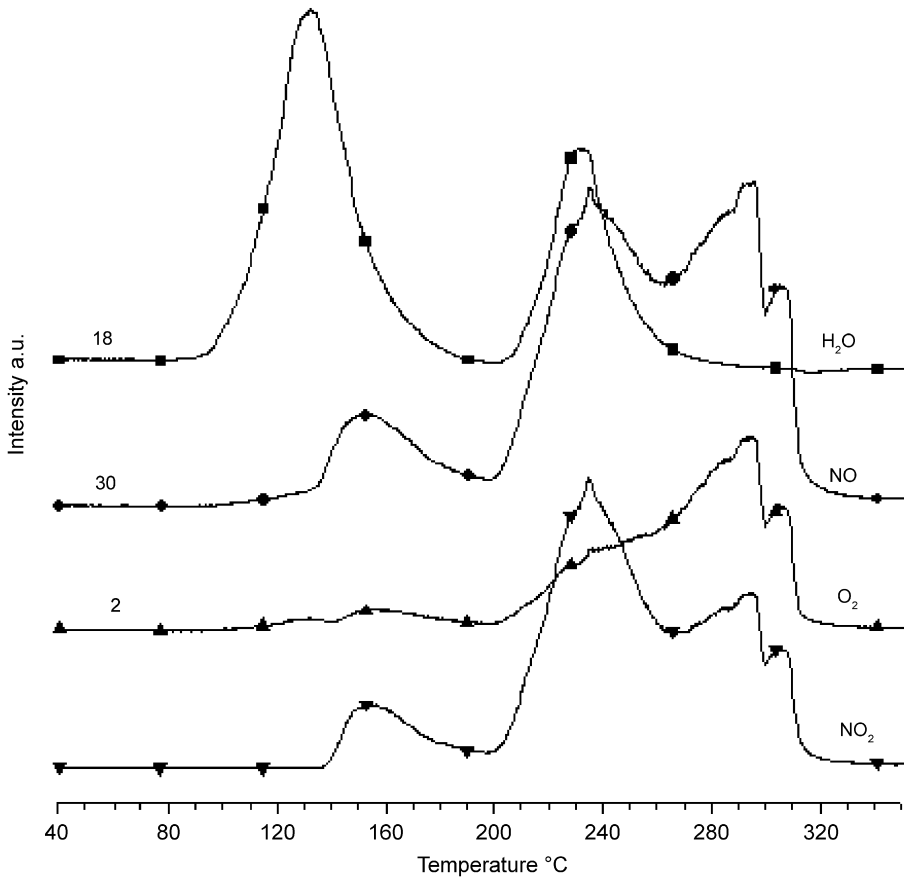

Fig. 9. Variation in ion current intensities of the gaseous products evolved during decomposition of Zn_1–H_2O. Collected for 0.05 g sample at a heating rate of 3 °C min^{-1} in flowing argon (10 ml min^{-1}).

Garcia-Martinez et al. [27] and Srivistava and Secco [28] investigated the thermal decomposition of $Zn_5(OH)_8Cl_2 \cdot H_2O$ and observed that the material decomposes to ZnO in three stages with the successive formation of $Zn_5(OH)_8Cl_2$, a mixture of ZnOHCl and ZnO, ZnO and anhydrous zinc chloride ($ZnCl_2$). Similarly, in their investigations on the thermal properties of $Zn_4(OH)_6SO_4 \cdot 5H_2O$, Ben'yash et al. [29] observed that the material decomposes to ZnO in four major stages with the successive formation of $Zn_4(OH)_6SO_4$, $Zn_2(OH)_2SO_4$ and ZnO, ZnO and anhydrous zinc sulphate ($ZnSO_4$) and finally the anhydrous zinc sulphate decomposing to ZnO and SO_3. ZnOHCl and $Zn_2(OH)_2SO_4$ like $Zn_3(OH)_4(NO_3)_2$ are layered and have zinc exclusively in octahedral coordination. It is however, important to note that the anhydrous zinc salts in these previous studies ($ZnCl_2$ and $ZnSO_4$) were well-crystallised products whereas the anhydrous zinc nitrate proposed in the present study is probably poorly crystallised. Although the structure of anhydrous zinc nitrate is not known, our PXRD and mass spectral data strongly suggest that it is formed as an intermediate in the thermal decomposition of zinc hydroxy nitrates. The formation of this poorly crystallised anhydrous zinc nitrate phase, therefore, explains the apparent discrepancy between mass spectral data and variable temperature data during decomposition of zinc hydroxy nitrates as reported from early studies.

4. Conclusions

The thermal decomposition of Zn_5–H_2O and Zn_1–H_2O has been re-examined. It has been demonstrated that despite the structural differences of the materials, they both decompose to ZnO via a poorly crystallised anhydrous zinc nitrate phase. The formation of this phase explains why earlier studies on these materials showed discrepancies between variable temperature XRD and TG analysis.

Acknowledgments

We acknowledge the Cambridge Commonwealth Trust and the Royal Society of London for financial support.

Appendix A. Supplementary materials

Supplementary data associated with this article can be found in the online version at doi:10.1016/j.jssc.2007.01.012.

References

[1] S.P. Newman, W. Jones, in: W. Jones, C.N.R. Rao (Eds.), Supramolecular Organization and Materials Design, Cambridge University Press, Cambridge, 2002, p. 295.

[2] M. Del Arco, E. Cebadera, S. Gutierrez, C. Martin, M.J. Montero, V. Rives, J. Rocha, M.A. Sevilla, J. Pharm. Sci. 93 (2004) 1649.
[3] M. Del Arco, S. Gutierrez, C. Martin, V. Rives, J. Rocha, J. Solid State Chem. 177 (2004) 3954.
[4] J.-H. Choy, M. Park, Clay Sci. 12 (2005) 52.
[5] S. Aisawa, H. Kudo, T. Hoshi, S. Takahashi, H. Hirahara, Y. Umetsu, E. Narita, J. Solid State Chem. 177 (2004) 3987.
[6] B.X. Li, J. He, D.G. Evans, X. Duan, Appl. Clay Sci. 27 (2004) 199.
[7] H. Tamura, J. Chiba, M. Ito, T. Takeda, S. Kikkawa, Solid State Ion 172 (2004) 607.
[8] C.L. Zhu, C.N. Chen, L.Y. Hao, Y. Hu, Z.Y. Chen, J. Cryst. Growth 263 (2004) 473.
[9] C.L. Zhu, C.N. Chen, L.Y. Hao, Y. Hu, Z.Y. Chen, Solid State Commun. 130 (2004) 681.
[10] S.M. Haile, D.W. Johnson, G.H. Wiseman, H.K. Bowen, J. Am. Ceram. Soc. 72 (1989) 2004.
[11] S.P. Naik, J.B. Fernandes, Thermochim. Acta 332 (1999) 21.
[12] C.P. Fah, J. Xue, J. Wang, J. Am. Ceram. Soc. 85 (2002) 273.
[13] E. Hosono, S. Fujihara, T. Kimura, H. Imai, J. Colloid. Interf. Sci. 272 (2004) 391.
[14] I. Kawai, Y. Sugahara, Y. Park, K. Kuroda, C. Kato, Ceram. Powder Sci. 22 (1991).
[15] M.S. Tokumoto, S.H. Pulcinelli, C.V. Santilli, V. Briois, J. Phys. Chem. B 107 (2003) 568.
[16] E. Hosono, S. Fujihara, T. Kimura, J. Mater. Chem. 14 (2004) 881.
[17] M. Louer, D. Louer, D. Grandjean, Acta Crystallogr., Sect. B: Struct. Sci. B 29 (1973) 1696.
[18] W. Stahlin, H. Oswald, Acta Crystallogr., Sect. B: Struct. Sci. B 26 (1970) 860.
[19] L. Eriksson, D. Louer, P.E. Werner, J. Solid State Chem. 81 (1989) 9.
[20] J.P. Auffredic, D. Louer, J. Solid State Chem. 46 (1983) 245.
[21] B. Malecka, R. Gajerski, A. Malecki, M. Wierzbicka, P. Olszewski, Thermochim. Acta 404 (2003) 125.
[22] S.P. Newman, W. Jones, J. Solid State Chem. 148 (1999) 26.
[23] V.C. Farmer (Ed.), The Infra-red Spectra of Minerals, Mineralogical Society, London, 1974.
[24] C.C. Addison, B.M. Gatehouse, J. Chem. Soc. (1960) 613.
[25] M.R. Waterland, A.M. Kelley, J. Chem. Phys. 113 (2000) 6760.
[26] R.A. Friedel, J.L. Schultz, A.G. Sharkey, Anal. Chem. 31 (1959) 1128.
[27] O. Garcia-Martinez, E. Vila, J.L.M. Devidales, R.M. Rojas, K. Petrov, J. Mater. Sci. 29 (1994) 5429.
[28] O.K. Srivastava, E.A. Secco, Can. J. Chem. 45 (1967) 579.
[29] E.Y. Ben'yash, V.I. Bulakhova, F.I. Vershinina, M.M. Shokarev, Russ. J. Inorg. Chem. 26 (1981) 888.